INFLUENCE OF TWISTED TAPE INSERT ON THE COOLANT FLOW CHARACTERISTICS IN SWIRLED FILM COOLING

***Vashista ADEMANE*[*1], *Ravikiran KADOLI*[1], *Vijaykumar HINDASAGERI*[2]**

[1]Department of Mechanical Engineering, National Institute of Technology Karnataka, Surathkal, Mangalore, Karnataka, India – 575025

[2]Department of Mechanical Engineering, KLS's Vishwanathrao Deshpande Institute of Technology, Haliyal, Karnataka, India – 570010

[*] Corresponding author; E-mail: v.ademane@gmail.com

The Present paper discusses film cooling behavior through numerical simulation in the presence of a twisted tape insert inside the film hole. The twisted tape insert imparts a swirl to the coolant flow. Coolant swirl intensity is controlled by varying the pitch of the twisted tape resulting in swirl numbers (S) of 0.0289, 0.116 and 0.168. The film cooling performance is evaluated using area-averaged effectiveness and heat transfer coefficient for blowing ratios of 0.5, 1.0, 1.5 and 2.0. Results revealed a significant amount of improvement in averaged effectiveness with the addition of swirl. Coolant swirl predominantly modifies the jet trajectory resulting in a reduced jet penetration and increased lateral expansion. Further investigation on the effect of twisted tape thickness on the coolant distribution has been found to be negligible. Pressure losses occurring due to the insertion of twisted tape inside the film hole is evaluated through the coefficient of discharge which indicated the necessity of higher pumping power than the film cooling case with no-swirl.

Keywords*: swirl film cooling, jet trajectory, twisted tape insert, effectiveness, blowing ratio*

1. Introduction

Achieving higher thermal efficiency to balance the energy demands in gas turbine engines necessitates higher turbine inlet temperature. This requires a better cooling mechanism for engine components. Film cooling is one such technique where coolant air is injected out of small holes situated over the surfaces as a protection against hot gases. Major parameters involved in controlling the film cooling behavior are injection angle, hole shape, blowing ratio, density ratio, hole length, mainstream turbulence, surface curvature, etc. [1].

In a film cooling situation, a transverse jet will be injected into a cross-flow which produces different types of vortical structures. Out of these vortices, counter rotating vortex pair (CRVP) adversely affect film cooling performance by lifting off the coolant jet away from the wall. Most of the recently proposed film cooling hole geometries mainly focus on reducing the effect of CRVP so that the jet stays closer to the wall. Bunker made an extensive review on shaped film holes out of which fan-shaped holes have proven to be the most effective in producing better cooling performance [2].

Recently computational tools are being used widely to develop different hole shapes to obtain better coolant distribution. In a recent study a combined hole configuration was numerically

investigated for film cooling with and without mist injection [3]. Further they extended their study to analyze the blockage effect by a spherical configuration [4]. Creating a semi-cylindrical trench in the upstream location of film cooling hole has showed an increase in effectiveness of around 30% [5]. There has been a constant effort in enhancing film cooling performance through novel film hole shapes such as coanda bump [6], vortex generator shapes [7], film holes embedded inside a trench [8]. Recently a study showed that the geometrical parameters involved in different hole shapes can be optimized to achieve a highest cooling performance [9].

Out of different parameters influencing film cooling mechanism, coolant swirl has been found to affect significantly the CRVP structure. Kavsaoglu and Schetz experimentally studied the effect of normal circular swirling jet with different swirling ratios and observed that the swirl causes asymmetries in the surface pressure distributions [10]. A study on scalar concentration transport of swirling transverse jet reported that the swirl has modified the symmetrical kidney-shaped mean concentration profile into a comma shape [11]. An Large Eddy Simulation (LES) study on a swirled normal jet observed that the asymmetry existed till x/d=8 at swirl number of 0.6 [12].

While preceding investigations are restricted to coolant injection normal to the cross-stream, the concept of introducing swirl has been extended to the case of slant angle injection such as film cooling. An experimental investigation on coolant swirl was studied by Takeishi et al. [13] in which two staggered impinging jets are positioned within the plenum chamber with a slant angle to produce swirled coolant flow inside the film hole. To further explore a detailed mechanism of coolant interaction with the cross-flow an LES study has also been performed [14]. Yang et al. performed a numerical analysis for the same arrangement as described in [13] for a cylindrical hole, a clover-shaped hole and a compound angled hole and found that a reduction in heat transfer in the case of compound angled holes [15]. A novel method for generating coolant swirl was investigated numerically by modifying the coolant entry into the film hole through the plenum chamber [16]. Out of three different chamber configurations studied, the third arrangement was found to increase the effectiveness by 550% for a blowing ratio of 1.5.

Very limited literature is available related to swirled film cooling and the mechanism used to generate the swirl in these works are more or less complicated. In this regard, the current paper makes a novel attempt to generate coolant swirl in the case of film cooling. In the present work, a twisted tape is inserted inside the film hole to generate the coolant swirl and the swirl intensity is controlled by varying the pitch of the twisted tape. The study has been performed with a numerical technique to explore the interaction mechanism between swirled coolant and cross flow. The cooling performance is evaluated through the area-averaged effectiveness and heat transfer coefficient and the consequence of swirl is examined by studying the flow structure at various locations of the flow field. Further the effect of various parameters such as blowing ratio, swirl number, twisted tape thickness and discharge coefficient are examined in the present work.

2. Numerical Modeling

2.1. Computational domain

Fig. 1 shows a three-dimensional computational domain used for the present work. The geometrical parameters are kept consistent with the experimental conditions used by Takeishi et al. [13]. The film cooling hole is having a diameter (d) of 5 mm with an inclination angle of 30° with

respect to the mainstream. Other geometrical parameters are fixed based on the film cooling hole diameter as shown in fig. 1. Co-ordinates x, y and z are non-dimensionalized using '*d*' and represented as *x/d*, *y/d* and *z/d* respectively. The origin is located at the trailing edge or the leeward side of the film hole. Coolant is made to enter the film hole through a plenum chamber placed below the film hole region.

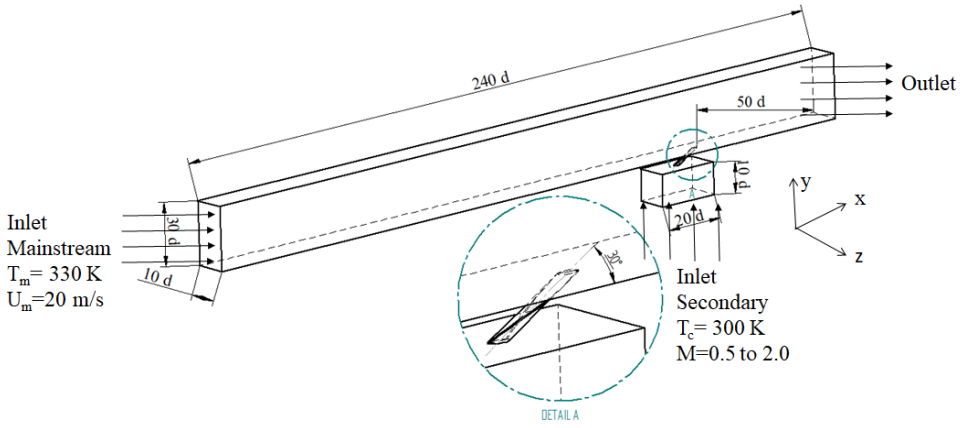

Figure 1. Three-dimensional view of the computational domain used for the numerical simulation

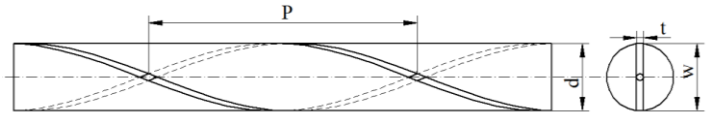

Figure 2. A two-dimensional view of twisted tape insert inside a pipe

Present work reports results of two cases. The base case is a simple cylindrical hole without a twisted tape insert and the second case is with a twisted tape insert inside the cylindrical film hole. A two-dimensional view of a pipe having a twisted tape insert is shown in fig. 2. The intensity of the coolant swirl is varied by imparting a tangential velocity to the coolant flow by changing the pitch of the twisted tape. Pitch is defined as the distance between two locations in the axial direction on the twisted surface corresponding to the 180° rotation of the twisted tape. The intensity of swirl is characterized by swirl number (S) which is defined in eq. (1) as the ratio of the axial flux of angular momentum to the axial flux of axial momentum [17].

$$S = \frac{G_\theta}{RG_x} = \frac{\int_0^R \rho V_x V_\theta r^2 dr}{R\int_0^R \rho V_x^2 r dr} \tag{1}$$

where V_x and V_θ are the axial and tangential velocities inside the pipe having a twisted tape and r is radial distance.

For the present case having twisted tape insert, the swirl number can be calculated in terms of twist ratio (*TR*) as given by eq. (2) [18],

$$S = \frac{\pi}{2K} \tag{2}$$

The twist ratio is a non-dimensional number defined as the ratio of pitch of the twisted tape to the width of the tape. Present work is based on the swirl numbers of 0.0289, 0.116 and 0.168.

2.2. Boundary conditions

The boundary conditions applied during the numerical simulation are given in tab. 1 along with other geometrical parameters which are in analogous to the experimental conditions. A uniform velocity and temperature inlet are applied at the mainstream inlet and the coolant is supplied from the bottom surface of the plenum chamber with a specified mass flow rate. The coolant mass flow rate is calculated through the required blowing ratio. The blowing ratio is defined as the ratio of coolant mass flux to the mainstream mass flux. The film cooling wall surface is maintained adiabatic with a no-slip boundary condition. The two sides and the top surface of the mainstream are given a symmetry boundary condition. For the case of heat transfer calculations, the adiabatic condition is changed to a surface with specified heat flux.

Table 1. Film cooling parameters used in the present study [13]

Parameters	**Values**
Mainstream velocity, U_∞	20 m/s
Mainstream Temperature, T_∞	330 K
Film hole diameter, d	5 mm
Hole length to diameter ratio, L/d	8
Injection angle, α	30°
Blowing ratio, M	0.5, 1.0, 1.5 and 2.0
Coolant inlet temperature, T_c	300 K
Turbulence intensity	0.36%

2.3. Numerical procedure

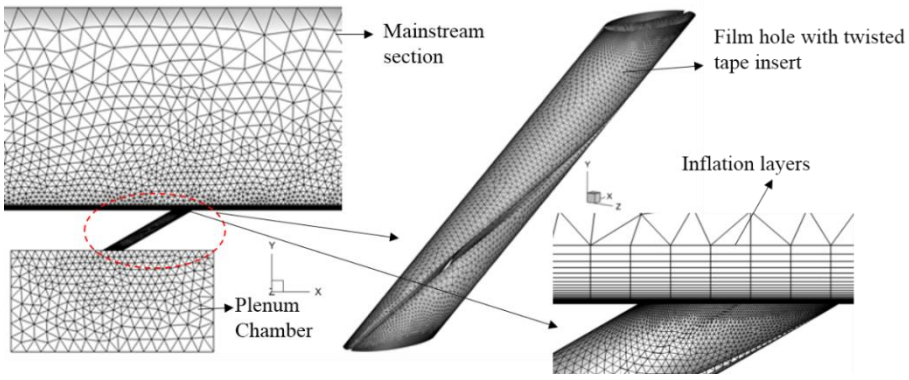

Figure 3. Computational mesh highlighting the film hole region with twisted tape insert

The computational domain is discretized using unstructured tetrahedral elements as shown in fig. 3 having inflation layers on the film cooled surface with a y+ value of less than 1. A three-dimensional numerical simulation is carried out using a finite volume based solver Ansys Fluent. Air as a working fluid with an ideal gas property is used. Reynolds Averaged Navier-Stokes equations are solved under steady-state conditions. Details of the governing equations, turbulence model and constants can be found in Ref. [19]. Convective terms are discretized with a second order upwind interpolation scheme. The pressure-velocity coupling is achieved through the SIMPLE algorithm. Turbulence quantities like kinetic energy and specific dissipation rate or dissipation are obtained using

SST k-ω, Std. k-ε, RNG k-ε and Realizable k-ε turbulence models. The converged solution is obtained after the residuals reached below 10^{-5} for continuity and momentum, 10^{-7} for energy and 10^{-4} for turbulence scalars.

3. Results and Discussion

3.1. Grid independence and validation

A grid dependency analysis was performed for the base case at a blowing ratio of 1.0 by considering four different mesh refinements of 1, 1.5, 2.2 and 4 million elements which are referred as Mesh-I, Mesh-II, Mesh-III and Mesh-IV respectively. Area averaged effectiveness are computed for these mesh refinements up to a length of x/d=20. The results are compared with the experimental data and the corresponding absolute error values are tabulated in tab. 2. Out of four mesh refinements studied, Mesh-I and Mesh-II are found to produce results having a close agreement with experimental data. Out of these two meshes, Mesh-II is selected for all further simulations because of the lowest error and having finer elements than Mesh-I.

Table 2. Area averaged effectiveness for different mesh refinements

Mesh Refinements	**Values**	**% Error**
Experimental result [13]	0.02372	-
Mesh-I	0.02174	8.30
Mesh-II	0.02255	4.89
Mesh-III	0.02676	12.85
Mesh-IV	0.02620	10.46

Table 3. $\bar{\eta}$ evaluated using different turbulence models on the downstream positions

Turbulence Models	***x/d*=2**	***x/d*=5**	***x/d*=10**	***x/d*=15**	***x/d*=20**
Experimental result [13]	0.0108	0.0275	0.0313	0.0251	0.0313
SST k-ω	0.0071 (34.4)	0.0200 (27.1)	0.0252 (19.35)	0.0253 (1.12)	0.0253 (19.18)
Std. k-ε	0.0272 (136.39)	0.0296 (8.77)	0.0322 (11.87)	0.0351 (53.87)	0.0379 (32.10)
Realizable k-ε	0.0255 (151.91)	0.0299 (7.80)	0.0350 (2.87)	0.0385 (40.05)	0.0413 (21.18)
RNG k-ε	0.0273 (152.49)	0.0298 (8.34)	0.0347 (11.03)	0.0389 (55.15)	0.0422 (34.76)

The fidelity of turbulence models in predicting numerical results are evaluated using four different turbulence models. Laterally averaged effectiveness is computed using SST k-ω, Std. k-ε, Realizable k-ε and RNG k-ε turbulence models for the base case at *M*=1.0. The effectiveness values are compared with experimental results at few selected downstream locations and tabulated in tab. 3. The percentage error between the experiment and the numerical model is mentioned inside the brackets. From tab. 3 it can be observed that the SST k-ω turbulence model is found to be

comparatively reasonable than other turbulence models. Even though other variants of k-ε turbulence models give better prediction at *x/d*=5 and 10, but the error values in the immediate downstream and far downstream (i.e, at *x/d*=2, 15 and 20) are very high. The average error value for the SST k-ω turbulence model is found to be around 20% while other models produce an error of more than 40%. Hence all further numerical calculations are conducted using the SST k-ω turbulence model.

Validation of the present numerical result is carried out by considering experimental data of Takeishi et al. [13] for a cylindrical hole film cooling without twisted tape insert. Fig. 4 shows the comparison of laterally averaged effectiveness for *M*=0.5 and 1.0. Result obtained using LES by Oda et al. [14] is also shown in fig. 4 for comparison. It is clear from the figure that the present numerical results have produced a fairly accurate prediction of effectiveness. Computed effectiveness distribution is in good agreement with the experimental results up to *x/d*=15. For *M*=1.0, an average deviation from the experimental data of around 0.5% is observed. In far downstream (*x/d*>15), the numerical result starts deviating and the effectiveness values are overpredicted. Such overprediction occurs due to more coolant accumulation near the wall as a result of a weak diffusion mechanism. The major source for this disparity is attributed to the isotropic eddy viscosity assumption used in predicting turbulence quantities. But when compared with the results of LES, present numerical results are found to be more accurate in predicting film cooling behavior.

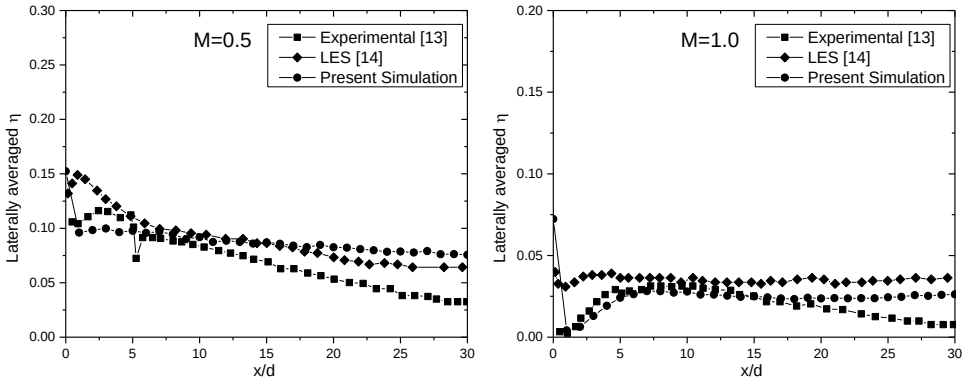

Figure 4. Validation of the present numerical results for *M*=0.5 and *M*=1.0

3.2. Effectiveness

The modification of coolant distribution due to swirl over the flat surface will be examined by the lateral dispersion of the coolant stream. Fig. 5 illustrates the effectiveness distributed laterally for a non-swirl case, fig. 5(a) and swirl case with swirl number of 0.168 fig. 5(b) at a few selected *x/d*s for *M*=1.0. Two important observations can be perceived by comparing the results of the two cases. The first observation is the peak effectiveness values which occur at the centerline at z/d=0. The centerline effectiveness for swirl case has been enhanced to almost double the values than a non-swirled case. Secondly, the lateral dispersion of the coolant is also improved by the swirled jet than the zero swirl case. It should be noted that the η distribution at *x/d*=20 for *S*=0 is less than at *x/d*=5 and 10 whereas for *S*=0.168 it is almost equal for *x/d*=10 and 20. This is basically due to the diffusion of a majority of the coolant lump while the jet is detached from the wall and the coolant concentration becomes weak when it reaches *x/d*=20. The swirled flow might have reduced the coolant mixing by keeping the jet close to the wall which may lead to achieving higher η values at *x/d*=20 for *S*=0.168 than the *S*=0 case. A trivial observation demonstrates that a symmetrical lateral distribution of η towards the *z/d*=0 plane

has now become asymmetrical with the imposition of swirl. The centerline η values are slightly moved towards –z direction for *S*=0.168 case.

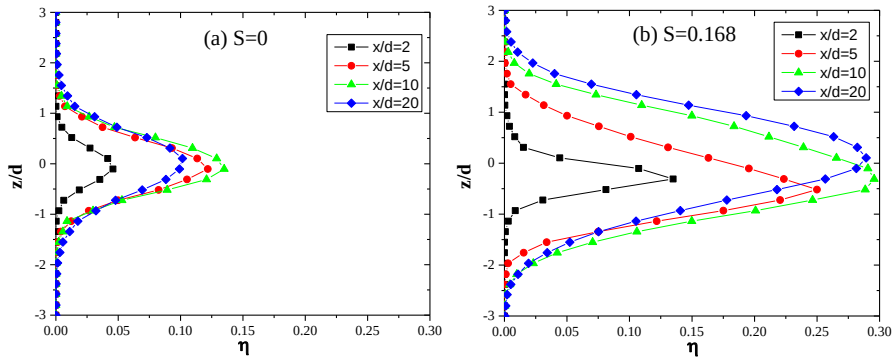

Figure 5. Lateral effectiveness distribution at downstream locations of the film hole

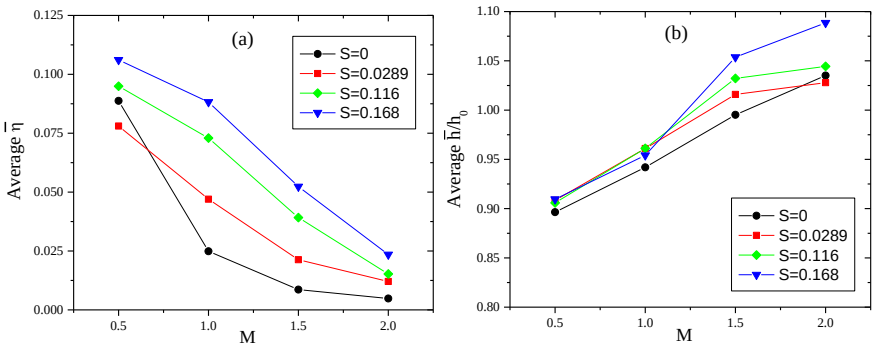

Figure 6. Area averaged film cooling (a) effectiveness (b) heat transfer coefficient for different swirl numbers and blowing ratios

A direct consequence from the results observed in fig. 5 is the improvement in the overall film cooling behavior which is given in terms of area averaged effectiveness as shown in fig. 6. Area averaged effectiveness is defined as the average effectiveness value evaluated over an entire film cooled surface. It can be evaluated as given below in eq. (3),

$$\bar{\bar{\eta}} = \frac{1}{x/d \times z/d} \int_{x/d=0}^{x/d=30} \int_{z/d=-3}^{z/d=3} \eta(x/d, z/d)\, d(z/d)\, d(x/d) \qquad (3)$$

Area averaged effectiveness corresponding to all the swirl numbers studied are plotted with respect to the blowing ratio in fig. 6(a). A clear observation is that the swirled film cooling produces higher effectiveness than non-swirled cases with higher $\bar{\eta}$ values with increase in swirl number. Average $\bar{\eta}$ gradually drops for higher blowing ratios due to the increased jet momentum resulting in coolant separation from the wall surface. The coolant swirl seems to have a minor effect on $\bar{\eta}$ at *M*=0.5 and 2.0 due to the lower momentum of the coolant jet in the former case. In the latter case i.e, at *M*=2.0, the coolant jet separation seems to dominate over the effect of swirl. It can be observed that the rate of increase in average $\bar{\eta}$ with *S* is high for *M*=1.0 compared to other blowing ratios which makes *M*=1.0 an optimum blowing ratio for operational engine conditions.

For the present film cooling design, the computed heat transfer coefficient values are normalized and averaged over the surface area and are plotted against *M* for different swirl numbers as shown in fig. 6(b). It can be seen that the heat transfer rate is proportional to the blowing ratio since

the increase in the blowing ratio amplifies the local turbulence levels. The addition of swirl to the coolant flow further enhances the disturbance in the mean flow causing a higher heat transfer rate for swirled cases than non-swirled cases.

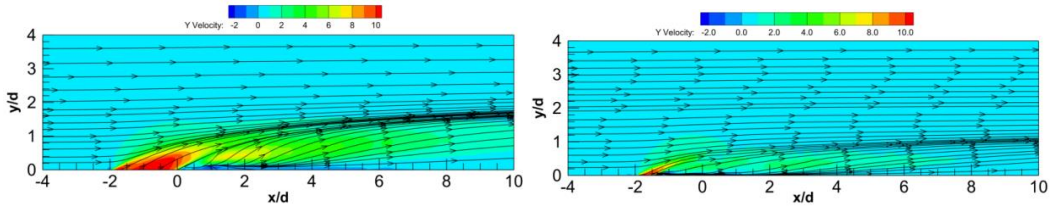

(a) *S*=0 **(b) *S*=0.168**

Figure 7. Streamlines on x-y plane at z/d=0 with y-velocity contour

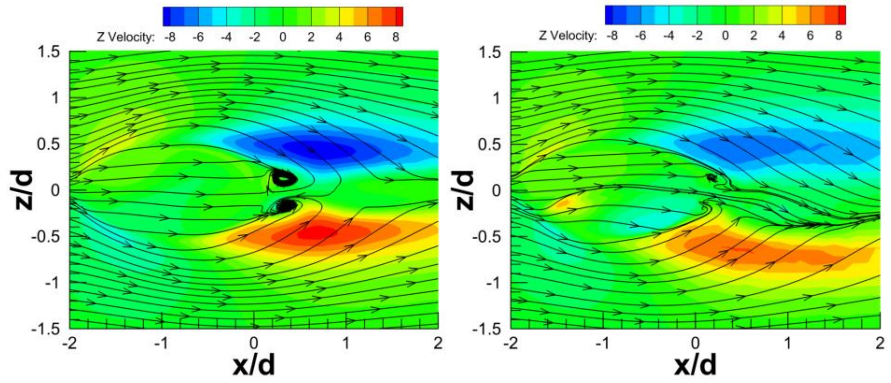

(a) *S*=0 **(b) *S*=0.168**

Figure 8. Streamlines on x-z plane at *y/d*=0.05 with z-velocity contour

The flow structures for swirled and non-swirled cases are shown in fig. 7 to fig. 9 with the help of streamlines and contour plots. When a coolant jet issues out from a film hole, it bends in the direction of free stream due to the stagnation pressure exerted by the cross flow. Non-swirled jet possesses a higher y-velocity component at the hole exit (fig. 7 (a)), which may lead to jet penetration and separation from the wall. The streamlines are getting squeezed from all the sides which accelerates the jet even further. Swirled flow, on the other hand, has a lower y-velocity component, as observed from fig. 7(b), due to twist insertion and tends to bend easily towards the cross-flow which makes them less likely to penetrate through the mainstream. When looking from the top view, fig. 8(a), there will be formation of wake vortices on the leeward side of the coolant jet because of the pressure gradient across the jet for the case of *S*=0. These vortices aid to the z-velocity component eventually leading to less lateral spreading. The twisted tape insert would not allow the formation of wake vortices behind the jet causing smaller z-velocity components (fig. 8(b)) and subsequently helping the jet to spread laterally.

CRVP is the major source for jet lift-off and detachment from the wall. It will augment the coolant-mainstream interaction and enhances the mixing by driving the mainstream towards the coolant jet core from lateral sides. As shown in fig. 9(a), CRVP constitutes of two symmetrical vortices rotating opposite to each other and travels downstream with the cross-flow for the case of cylindrical hole film cooling having zero swirl. Inserting twisted tape inside the film hole mainly divides the coolant jet into two lobes with one being smaller than the other. The induced swirl yields an asymmetrical CRVP structure, as shown in fig. 9(b), in which two vortices will have different

strengths of rotation. Reduced vortex interaction at the center plane (z/d=0) keeps the jet closer to the wall and the vortex having a bigger size helps in spreading the coolant laterally. It can also be observed from fig. 9(b) that there is a formation of secondary vortex in the downstream (at x/d=10, S=0.168), which might further suppress the strength of the main vortex and aids in better spreading.

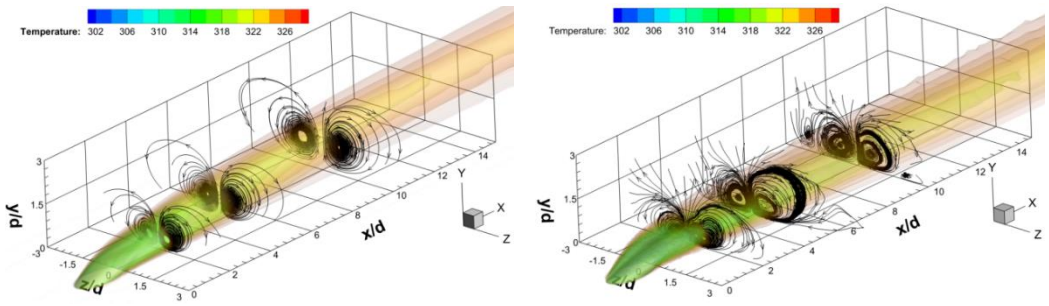

(a) S=0 **(b) *S*=0.168**

Figure 9. Three-dimensional iso-contours of temperature along with streamlines on y-z plane at *x/d*=2, 5 and 10

3.3. Jet trajectory

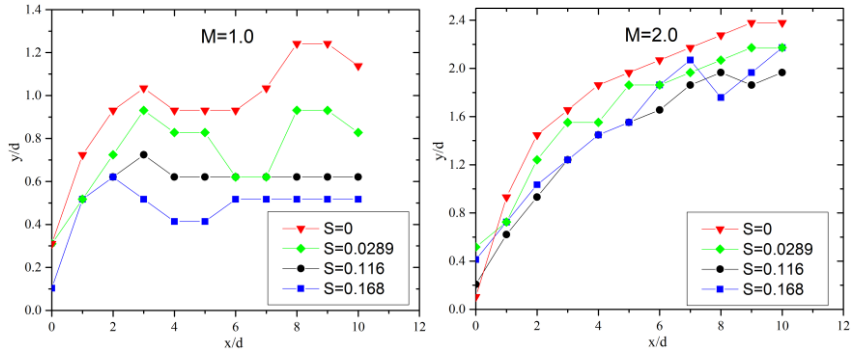

Figure 10. Comparison of observed jet trajectory for different swirl numbers

The extent of coolant jet penetration into the mainstream can be characterized by calculating the jet trajectory. Different methods have been followed in the literature to calculate the jet trajectory [20]. In the present paper, the jet trajectory is calculated by finding the minimum value of the local scalar concentration in x-y plane at z/d=0. The jet trajectories for different swirl numbers are plotted in fig. 10 for blowing ratio of 1.0 and 2.0. It is obvious that with increase in blowing ratio (from M=1.0 to M=2.0) there will be deeper jet penetration. But the advantage of having a swirled flow over a non-swirled case can be clearly observed by looking at the reduction in jet penetration height. As compared to non-swirled flow, the swirled flow (S=0.168) has reduced the penetration height of up to 48% and 22% for M=1.0 and 2.0 respectively. At a higher blowing ratio (M=2.0), the penetration height does not seem to reduce beyond a certain limit with increase in swirl number. This could be due to the higher jet momentum which is dominating over the effect of swirl.

3.4. Effect of twisted tape thickness

The numerical simulations so far have been conducted by considering twisted tape at a thickness of 0.5mm. But it is essential to study the influence of twisted tape thickness on the coolant

distribution. Hence a parametric study is conducted by considering the twisted tapes having a thickness of 0.5mm, 0.25mm and 0.1mm. There is no particular reason behind selecting these three values. But a thick tape might lead to blocking of the coolant through the film hole and increase pressure drop across the hole. Hence a maximum thickness of 0.1d and a minimum value of 0.02d are considered. Laterally averaged effectiveness evaluated at S=0.168 and M=1.0 for these three thickness cases are shown in fig. 11. There is no significant variation in the computed $\overline{\eta}$ is observed within the range of thickness studied. Only for the case of t=0.1mm, a slight decline in the value of $\overline{\eta}$ for x/d<3 and increase of around 7% is observed for x/d>15.

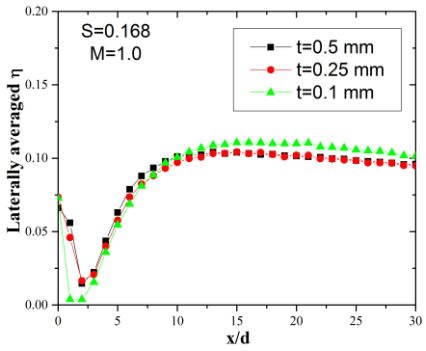

Figure 11. Twisted tape thickness effect on the effectiveness

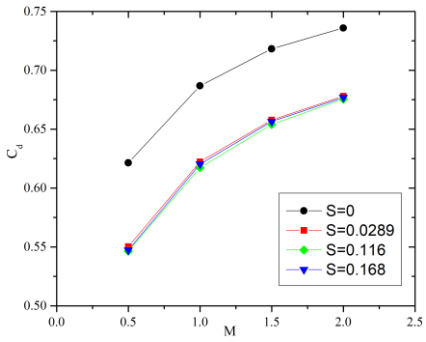

Figure 12. Discharge coefficient for the case of with and without twisted tape insert

3.5. Coefficient of discharge

Inserting twisted tape could lead to the requirement of extra pumping power to eject the coolant through the hole. Discharge coefficients illustrate the pressure losses occurring through the film hole and it is defined as the ratio of actual mass flow rate to the theoretical mass flow rate. The theoretical mass flow rate can be obtained by measuring the pressure losses occurring between the inlet and exit of the film hole. The discharge coefficient can be calculated using eq. (4) as:

$$C_d = \frac{\dot{m}_c}{\frac{\pi d^2}{4}\sqrt{2\rho_c(p_c^* - p_\infty)}} \tag{4}$$

Fig. 12 shows the discharge coefficient obtained using eq. (4) for different blowing ratios and swirl numbers. It appears that the value of C_d has reduced approximately 7% - 11% for swirled flow cases than non-swirled flows. This is the direct consequence of increased frictional losses inside the film hole due to the presence of twisted tape. The twisted tape necessitates additional pumping power to inject the coolant. But the twist ratio does not appear to affect C_d, since the length of the twisted tape is the same for all three swirl numbers. It is recommended that one has to optimize the blowing ratio and the pumping power to obtain maximum efficiency.

4. Conclusions

The present work has reported the effect of coolant swirl on the film cooling behavior of a circular hole with a twisted tape insert. Three swirl numbers are investigated for blowing ratios of 0.5 to 2.0 and compared with a non-swirl case. Results presented in terms of area-averaged effectiveness revealed that the film cooling with twisted tape insert is able to enhance the cooling

performance by up to 250% for an optimum blowing ratio at S=0.168. Even though an improvement in $\bar{\eta}$ of around 380% is observed for M=2.0 at S=0.168, a higher heat transfer rate limit the applicability of swirl at high blowing ratios. Analyzing the flow structure has demonstrated that the induced swirl mainly creates an asymmetry in the flow resulting in a better lateral spreading of the coolant. It is also noted that the jet penetration height has been reduced by around 48% due to the influence of swirl. The twisted tape thickness does not appear to affect the coolant distribution drastically. The discharge coefficient for the case of twisted tape insert is obtained to be lower than a simple cylindrical hole film cooling case which may require additional pumping power.

Nomenclature

C_d	Co-efficient of discharge		**Greek Symbols**
d	Diameter of the film hole [m]	α	Injection angle
G	Axial flux of momentum	η	Effectiveness = $(T_{aw}-T_m)/(T_c-T_m)$
h	Heat transfer coefficient [$Wm^{-2}K^{-1}$]	θ	Tangential component
K	Twist ratio	ρ	Density [kgm^{-3}]
M	Blowing ratio = $\rho_c U_m/\rho_c U_m$	ϕ	Non-dimensional metal temperature
$\dot{m}$	Mass flow rate [kgs^{-1}]	ω^*	Non-dimensional vorticity
P	Pitch of the twisted tape [mm]	ω	Vorticity component [s^{-1}]
p	Pressure [Pa]		**Subscripts**
q''	Heat flux [Wm^{-2}]	aw	Adiabatic wall
R	Radius [m]	c	Coolant
r	Radial distance [m]	f	Film cooling
S	Swirl number	m	mainstream
T	Temperature [K]	0	Non-film cooling
t	Twisted tape thickness[mm]	w	Wall
U	Velocity [ms^{-1}]		**Superscript**
W	Width of the twisted tape [mm]	$\bar{}$	Laterally averaged quantity
x,y,z	Co-ordinate directions		**Abbreviations**
		CRVP	Counter rotating vortex pair
		LES	Large eddy simulation
		NHFR	Net heat flux reduction

References

[1] Han, J.-C., et al., *Gas Turbine Heat Transfer And Cooling Technology, Second Edition*, 2012

[2] Bunker, R.S., A Review Of Shaped Hole Turbine Film-Cooling Technology, *J. Heat Transfer*, *127* (2005), 4, pp. 441

[3] Tian, K., et al., Effect Of Combined Hole Configuration On Film Cooling With And Without Mist Injection, *Therm. Sci.*, *22* (2018), 5, pp. 1923-1931

[4] Wang, J., et al., Effect Of Spherical Blockage Configurations On Film Cooling, *Therm.*

Sci., 22 (2018), 5, pp. 1933-1942

[5] Ravi, D., Parammasivam, K.M., Enhancing Film Cooling Effectiveness In A Gas Turbine End-Wall With A Passive Semi Cylindrical Trench, *Therm. Sci., 23* (2019), 3, pp. 2013-2023

[6] Uk, J., et al., Optimization Of The Coanda Bump To Improve The Film Cooling Effectiveness Of An Inclined Slot, *Int. J. Therm. Sci., 139* (2019), February, pp. 376-386

[7] Zheng, D., et al., Numerical Investigation On The Effect Of Vortex Generator Shapes On Film Cooling Performance, *Thermophys. Aeromechanics, 26* (2019), 3, pp. 455-460

[8] Barahate, S.D., Vedula, R.P., Film Cooling Performance Measurement Over A Flat Plate For A Single Row Of Holes Embedded In An Inclined Trench, *Int. J. Therm. Sci., 150* (2020), December 2019, pp. 106215

[9] Taheria, Y., et al., Multi-Objective Optimization Of Three Rows Of Film Cooling Holes By Genetic Algorithm, *Therm. Sci.*, (2020), 0, pp. 230-230

[10] Kavsaoglu, M.S., Schetz, J.A., Effects Of Swirl And High Turbulence On A Jet In A Crossflow, *J. Aircr., 26* (1989), 6, pp. 539-546

[11] Niederhaus, C.E., et al., Scalar Transport In A Swirling Transverse Jet, *AIAA J., 35* (1997), 11, pp. 1697-1704

[12] Denev, J.A., et al., Structure and mixing of a swirling transverse jet into a crossflow, *Proceedings*, 4th International Symposium on Turbulence and Shear Flow Phenomena, 2005, pp. 1255-1260

[13] Takeishi, K., et al., Film Cooling With Swirling Coolant Flow, *WIT Trans. Eng. Sci., 68* (2010), pp. 189-200

[14] Oda, Y., et al., Large Eddy Simulation Of Film Cooling With Swirling Coolant Flow, *ASME/JSME Therm. Eng. Jt. Conf., 38921* (2011), pp. T10102

[15] Yang, X., et al., Numerical Analysis On Effects Of Coolant Swirling Motion On Film Cooling Performance, *Int. J. Heat Mass Transf., 90* (2015), pp. 1082-1089

[16] Jiang, Y., et al., Investigation On Film Cooling With Swirling Coolant Flow By Optimizing The Inflow Chamber, *Int. Commun. Heat Mass Transf., 88* (2017), September, pp. 99-107

[17] Ashwani K. Gupta, D. G. Lilley, N.S., *Swirl Flows*, Abacus Press, 1984

[18] Kumar, S.S., et al., Local Heat Transfer Distribution On A Flat Plate Impinged By A Swirling Jet Generated By A Twisted Tape, *Int. J. Therm. Sci., 111* (2017), pp. 351-368

[19] ANSYS Inc., *ANSYS FLUENT Theory Guide*, ANSYS FLUENT 16.0.0, Cononsburg, PA, USA, 2014

[20] Mahesh, K., The Interaction Of Jets With Crossflow, *Annu. Rev. Fluid Mech., 45* (2013), pp. 379-407

Received: 01.05.2021.

Revised: 22.07.2021.

Accepted: 26.07.2021.